PERGAMON

Journal of Structural Geology 25 (2003) 59–78

JOURNAL OF STRUCTURAL GEOLOGY

www.elsevier.com/locate/jsg

Internal structure and permeability of major strike-slip fault zones: the Median Tectonic Line in Mie Prefecture, Southwest Japan

Christopher A.J. Wibberley*, Toshihiko Shimamoto

Department of Geology and Mineralogy, Division of Earth and Planetary Sciences, Graduate School of Science, Kyoto University, Kyoto 606-8502 Japan

Received 2 March 2001; accepted 10 January 2002

Abstract

Fault zone structure and permeability data from the Median Tectonic Line (MTL) in Mie Prefecture, Southwest Japan suggest that fault permeability models are currently too simplistic for such large structurally complex fault zones. Ryoke Belt mylonites are cut by mineralised brittle structures up to 300 m North of the MTL that show evidence of fluid circulation. The Sambagawa schist on the south side of the MTL is deformed into foliated quartz/phyllosilicate gouge across a 15-m-wide zone. The complex fault contact area has foliated cataclasite up to 4 m wide, and is cut by a narrow central planar slip zone that probably represents the most recent seismogenic principal displacement zone. Laboratory-determined permeability data show wide variation with fault rock microstructure (e.g. gouge microclast size), controlled by structural position in the fault zone and slip zone intersections. Central slip zone gouges have the lowest permeabilities of all of the fault rocks studied. Fault permeability models should take into account asymmetry where widely contrasting protolith lithologies exist and large permeability variations within a complex central fault zone 'core'. Pore pressure evolution during rupture propagation may vary greatly because of this complexity, but thermal pressurisation is feasible above certain pressures if the slip remains within fine-grained gouge. The different deformation behaviours of contrasting protolith lithologies control the fault zone fabrics and hence final permeability structure.

Keywords: Fault; Permeability; Cataclasite; Gouge; Fluid flow; Strength

1. Introduction

Fluid flow is an important geological process because it strongly affects metamorphism and deformation processes within the Earth's crust (e.g. Etheridge et al., 1983; Hickman et al., 1995). Large crustal fault zones are important in controlling fluid flow because of their known ability to act as conduits and/or barriers during their history of activity and inactivity (e.g. Fyfe et al., 1978; Kerrich, 1986; McCaig, 1988; Sibson, 1992). However, large fault zones have complicated structures, which depend on the history of the fault, the protoliths and the range of conditions throughout which the fault has experienced deformation. All of these affect the structure and distribution of fault rocks and their physical properties (e.g. Chester and Logan, 1986; Seront et al., 1998), making the understanding and prediction of fluid flow difficult. Yet the evolution of fluid pressures during the seismic cycle on active faults (e.g. Sibson, 1992; Muir-Wood, 1994), and transient changes in permeability behaviour of inactive faults during nearby seismic activity (e.g. King et al., 1999) could both in the future be of practical use in earthquake prediction. Models invoking fluid pressure-controlled fault weakening and earthquake slip instability for example (e.g. Sibson, 1973; Lachenbruch, 1980; Mase and Smith, 1987; Byerlee 1990; Rice, 1992) require data on permeability structure of major fault zones. Particular problems of how permeability varies within the fault zone due to the distribution of different fault rocks, and variation with pressure in the seismogenic layer need to be addressed. Such data are scarcely available for permeability studies placed in a well-defined structural context within major fault zones.

Permeability data for fault gouge from the San Andreas fault (e.g. Chu et al., 1981; Morrow et al., 1984), the Carboneras fault (Faulkner and Rutter, 1998) and the Nojima fault (Lockner et al., 1999; Mizoguchi et al., 2000) all show relatively low values between 10^{-18} and 10^{-22} m^2 at effective pressures of between 50 and 180 MPa. Such data suggest the likely barrier to transverse fluid flow that fault gouge can provide. Previous permeability data across entire fault zones suggest that

* Corresponding author. Tel.: +81-75-753-4266; fax: +81-75-753-4189.
E-mail address: cwibber@ip.media.kyoto-u.ac.jp (C.A.J. Wibberley).

0191-8141/02/$ - see front matter © 2002 Published by Elsevier Science Ltd.
PII: S0191-8141(02)00014-7

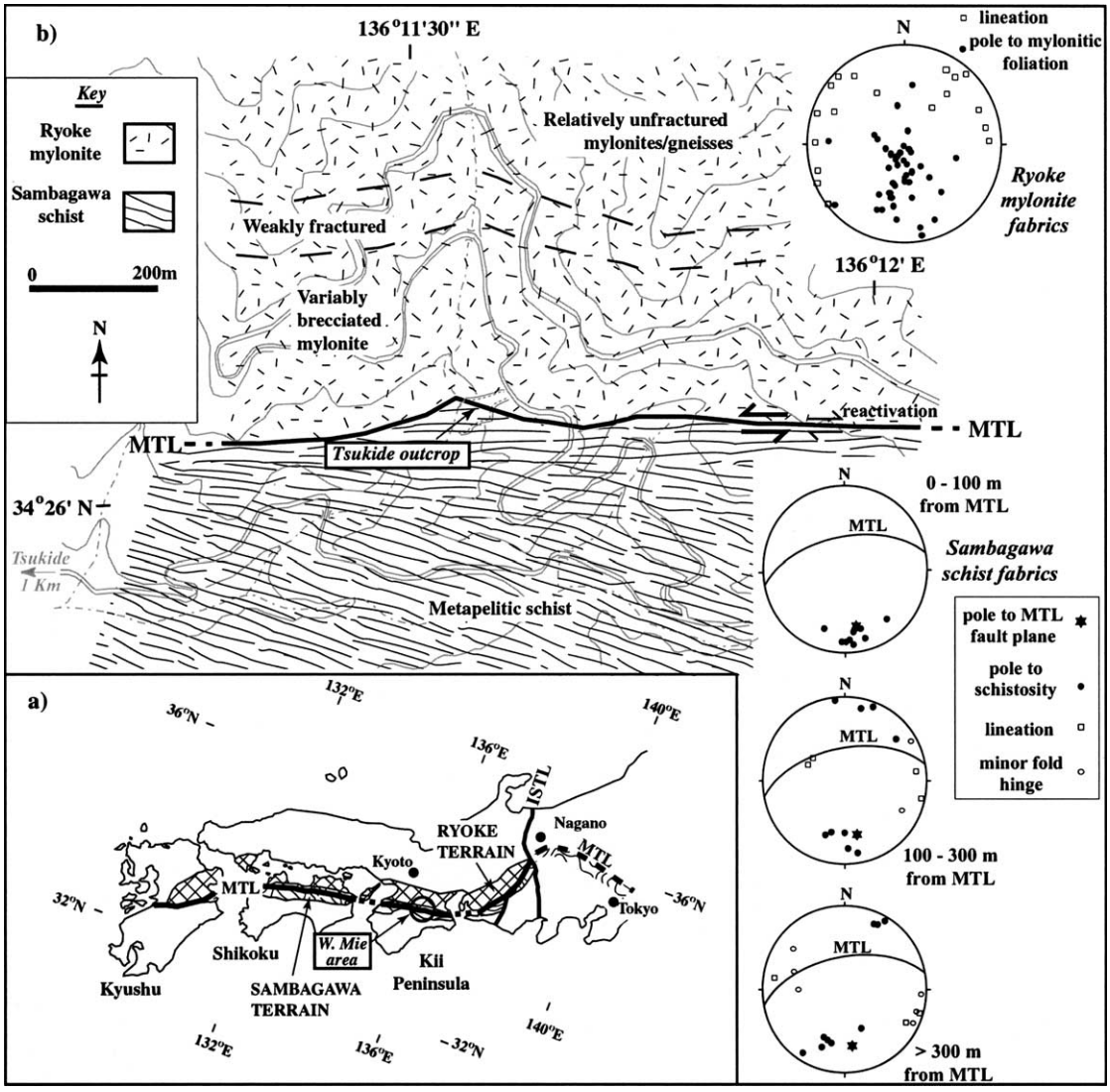

Fig. 1. (a) The Median Tectonic Line (MTL) and adjacent tectonic units in SW Japan. ISTL denotes the Itoigawa–Shizuoka Tectonic Line. (b) Geological map of the Median Tectonic Line near Tsukide, western Mie Prefecture, including structural data on the deformation fabrics around the Median Tectonic Line. The stereograms are lower-hemisphere equal-area stereographic projections.

the permeability of the protolith becomes significantly enhanced around the fault by a zone of fracture damage, but decreases into a core zone of fault gouge (Evans et al., 1997; Seront et al., 1998). Such previous work tended to focus on structurally simple cases in order to compile these models (e.g. by Caine et al., 1996), such as a single protolith like a structurally isotropic granite on both sides of the fault. In this paper, the aim is to further these previous ideas by incorporating new room temperature permeability data on a structurally more complex yet nevertheless realistic fault zone, using the Median Tectonic Line in Southwest Japan for the study. Future studies of higher temperature permeability and the effect of shear deformation are intended to compliment the present work in order to construct fault rock dynamic permeability models across the entire middle to upper crust.

2. The Median Tectonic Line in Mie Prefecture

2.1. Geological setting

The Median Tectonic Line (MTL) is the tectonic discontinuity separating the Ryoke low-P/high-T metamorphic terrain from the Sambagawa high-P/low-T metamorphic terrain throughout Southwest Japan (Fig. 1a). The MTL is Japan's largest onshore exposed fault, with a displacement history dating back at least to the early Cretaceous (e.g. Ichikawa, 1980). The magnitude of MTL displacement is difficult to estimate and poorly constrained in the order of around 200–1000 km. The present day MTL is a high angle fault at outcrop, separating the Ryoke granitic gneisses and mylonites in the North from the Sambagawa metapelitic and metapsamitic schists in the South (Fig. 1a). However, the origin and early juxtaposition history of the fault are

Table 1
Zonation of fault rock types across the Median Tectonic Line fault zone at the Tsukide outcrop, western Mie Prefecture. Some of the data on timing and conditions of fault rock generation are drawn from Shimada et al. (1998), Takagi et al. (1989) or related to young events dated by Sugiyama (1992)

Origin	Derived from Ryoke Belt				Derived from Sambagawa Belt		
Fault rock zone	A—Ryoke mylonite	B—Variably fractured mylonite	C—Fractured phyllosilicate-rich mylonite	D—Cataclasites	E—Central slip zone	F—Sambagawa-derived foliated gouges	G—Sambagawa schist
Distance	> 10 m North	300–10 m North	10–4 m North	4–0 m North	0–0.1 m South	0.1–15 m South	> 15 m South
Deformation structures	Mylonitic foliation	Epidote veins and open fractures, breccia zones often epidote-cemented, occasional cemented cataclasite bands. Heterogeneous distribution	Feldspar fracturing on northern edge with chlorite in-fills. Remainder predominantly aligned chlorite fabric with quartz cemented zones, cut by calcite veins and open fractures	Anastomosing fracture schistosity and/or foliated cataclasite fabrics, in places cemented, cut by subsidiary faults	Scaley clay-rich gouge fabric	Foliated gouge with quartz microclasts and occasional macroclasts of cemented quartz breccia. Deformation localised into Riedel shear zones	Metapelitic schistosity of mica and annealed quartz domains, occasional unconnected faults and fractures
Deformation mechanisms	Crystal plastic	Fracture, cataclasis	Microfracturing → fluid-assisted creep, cataclasis	Fracturing, cataclasis and cataclastic flow	Comminution and/ or hydroplasticity	Comminution and cataclastic flow	Crystal plastic, DMT, localised later fracture
Kinematics	Top-to-the-South reported elsewhere. Sinistral/top-to-the-West evidenced in field area and reported elsewhere	Few data available	Sinistral East–West strike-slip	Mainly sinistral East–West strike-slip, some late dextral slip bands close to the central slip zone cutting oblique subsidiary faults	East–West strike-slip on a plane dipping approx. 60° North	Mainly sinistral East–West strike-slip, including Riedel shear zones, with evidence for dextral reactivation close to the central shear zone	Initial fabric has unconstrained kinematics. Passive rotation of schistosity up to 300 m from MTL is consistent with sinistral shear
P–T conditions	10–15 km depth and 500 → 300 °C	Retrogressive conditions at shallow greenschist grade	Feldspar retrogression to chlorite suggests probably lower greenschist	Poorly constrained but iron-stained precipitate suggests meteoric water circulation and oxidation	Timing suggests very shallow (0–1 km?) depths	Very poorly constrained within the depth range 10 → 1 km	High P/Low T schist with progressive deformation at shallowing conditions
Chronology	Mid-late Cretaceous top-to-the-South, latest Cretaceous sinistral strike slip	Fracturing post-Cretaceous	Post-early Cretaceous to early Palaeogene	Post-dates phyllosillicate-rich mylonite	Youngest structure, probable Pliocene	Palaeogene with later localisation through to Pliocene	Late Cretaceous
Suggested relative timing (1 → 5)	1,2	3	2,3	4	5	4 to 5	1 to 2

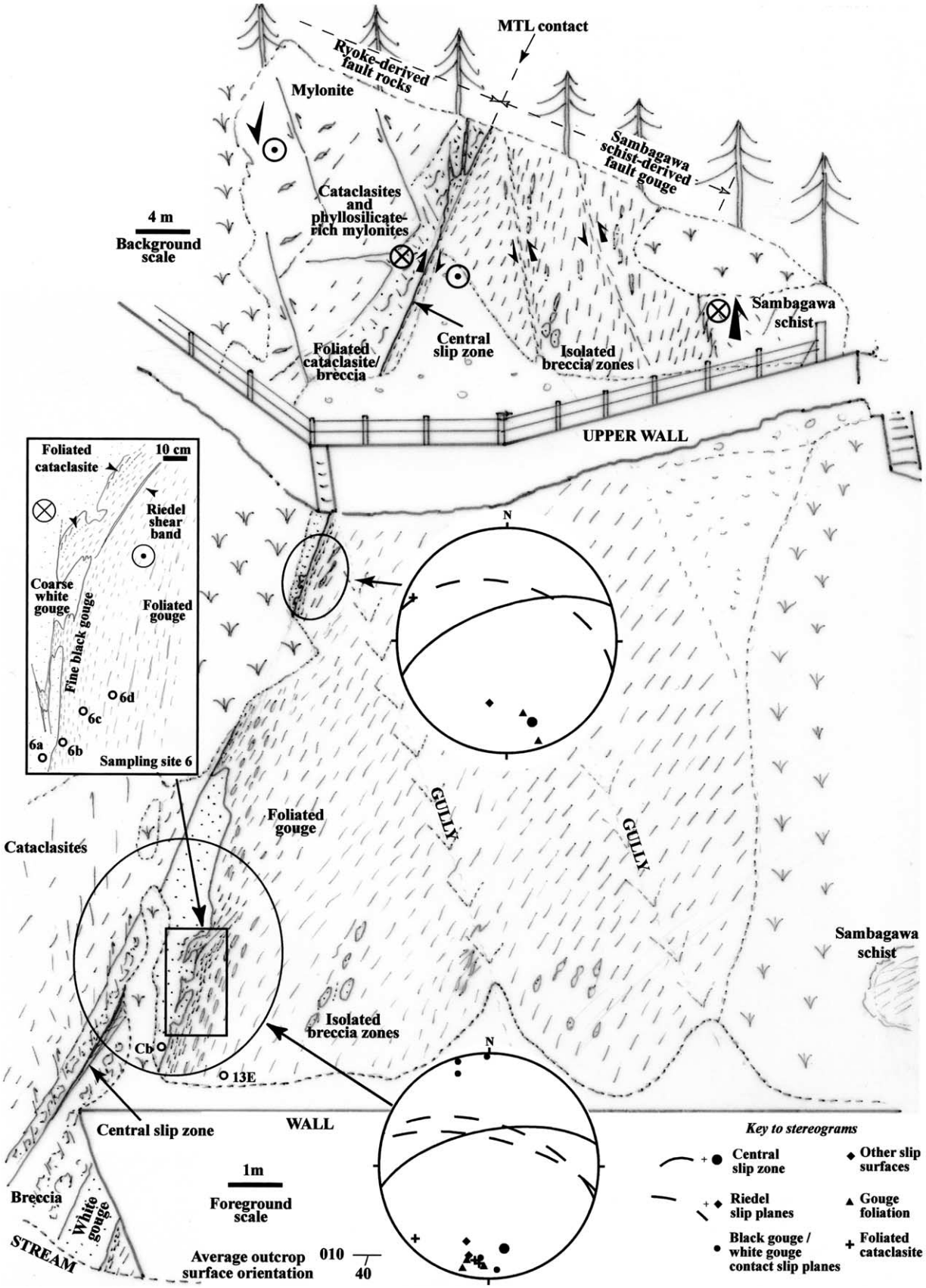
MTL contact
Ryoke-derived fault rocks
Mylonite
Sambagawa schist-derived fault gouge
4 m
Background scale
Cataclasites and phyllosilicate-rich mylonites
Central slip zone
Foliated cataclasite/ breccia
Isolated breccia zones
Sambagawa schist
UPPER WALL
Foliated cataclasite
10 cm
Riedel shear band
Coarse white gouge
Foliated gouge
Fine black gouge
6d
6c
6a
6b
Sampling site 6
N
GULLY
GULLY
Foliated gouge
Cataclasites
Sambagawa schist
Isolated breccia zones
Cb
13E
N
Central slip zone
WALL
1m
Foreground scale
Breccia
White gouge
STREAM
Average outcrop surface orientation 010 / 40
Key to stereograms
Central slip zone
Other slip surfaces
Riedel slip planes
Gouge foliation
Black gouge / white gouge contact slip planes
Foliated cataclasite

different from the present day picture (e.g. Hara et al., 1980), and not fully understood.

Mylonites exposed on the north side of the MTL consistently show evidence for sinistral shear, which is thought to have predominated from the late Cretaceous to mid-Tertiary (e.g. Takagi et al., 1989; Shimada et al., 1998), possibly overprinting earlier top-to-the-South structures (Ohtomo, 1993; Sakakibara, 1995). Such important strike-slip deformation on the MTL reworked the original Ryoke mylonites and Sambagawa schists to generate a variety of different fault rocks, such as foliated cataclasites, random-fabric cataclasites/breccias, and gouges (e.g. Takagi, 1985, 1986). The presence of the cataclastic fault rocks localised on or close to the MTL, overprinting a wide mylonite zone, has been interpreted to signify continued strike-slip deformation on the MTL at progressively shallower crustal conditions (Takagi, 1986).

In the Kii Peninsula (Fig. 1a) and further West, the MTL has accommodated additional much younger (Miocene onwards) deformation by dextral reactivation. The onset and cessation of this reactivation has been migrating westward through Southwest Japan (Sugiyama, 1992). The MTL in western Kii Peninsula and Shikoku is currently active, whilst in eastern Kii Peninsula, including the study area, it is now inactive.

2.2. Fault zone structure

2.2.1. Regional structure

In western Mie Prefecture (Fig. 1) the MTL is defined by a sharp contact, dipping 65° to the North, between Ryoke-derived fault rocks (mainly cataclasites) on the north side and Sambagawa-derived fault rocks (mainly black foliated gouge) on the south side (Table 1). The Ryoke mylonites are deformed and altered to phyllosilicate-rich mylonites up to 10 m North of the present MTL fault contact, beyond which the original mylonite fabric with feldspar porphyroclasts is visible. Fractures, epidote and quartz veins, cohesive cemented microbreccias and cemented cataclasite zones overprint the mylonite fabrics in a zone of brittle deformation up to 300 m North of the MTL contact. Despite the heterogeneity typical of brittle deformation, a general increase in cataclastic overprinting intensity and degree of mineralisation occurs towards the MTL. The Sambagawa metapelitic quartz–mica schist on the south side of the MTL shows a general swing in foliation orientation towards the fault, consistent with passive rotation of the schistosity during sinistral strike-slip movement on the MTL (Fig. 1b). Relatively small isolated faults with gouge zones up to 0.1 m wide are occasionally present, even several hundred metres South of the MTL.

2.2.2. Detailed outcrop data

Mapping at a particularly spectacular outcrop close to the village of Tsukide ('Moonrise') shows that the Sambagawa schist has been deformed into black foliated gouge across an approximately 15-m-wide zone (Fig. 2; Table 1). Within this foliated gouge zone, the fabric swings towards the orientation of a central slip zone (see stereogram data in Fig. 3). Localised rotation and intensification of this gouge fabric into R_1 Riedel shear zones (e.g. Logan et al., 1992) is evidenced (Fig. 3). Both the swing in fabric orientation and the Riedel shear kinematics are compatible with formation during the main sinistral shear event on the MTL fault zone. Late Tertiary-to-Recent dextral activity does not appear to have significantly modified the general orientations of earlier structures. Closely associated with these Riedel shear zones are clasts of fractured, calcite-cemented quartz cataclasite within the black gouge matrix, locally forming isolated breccia lenses.

The central slip zone (Figs. 2 and 3) is a strikingly planar 50–100 mm wide slickenside-bound zone of extremely fine black gouge that truncates all adjacent structures. On the North side of the central slip zone, foliated cataclasite up to 4 m wide is composed of aligned clasts or layers of coarse quartz gouge mixed with a black phyllosilicate gouge, suggesting mixing of fault rocks from the two sides. Close to the central slip zone, fabrics in the foliated cataclasite such as quartz gouge tails deflected around larger clasts, and low-angle Riedel slip surfaces suggest deformation by dextral shear. However, fabrics further away from the central slip zone suggest deformation during sinistral shear. This indicates that foliated cataclasite was generated during the late phases of sinistral shear on the MTL, but strain localised within it during the relatively recent dextral movement on the MTL.

The contact between the foliated cataclasites and the black gouge is not uniformly planar, although for much of the length of the outcrop it is defined by the continuous planar central slip zone. Although narrow central slip zones have been described from other large strike-slip fault zones (e.g. Chester and Chester, 1998), much more lateral variability exists here due to additional structural complexities close to the centre of the MTL fault zone. These complexities have arisen due to slip on oblique subsidiary slip zones in the Ryoke-derived fault rocks, possibly intermittent with slip on MTL-parallel fault surfaces. Slip on these oblique minor faults has offset many of the fault rocks (Fig. 3), but most of them have not significantly affected the poorly consolidated foliated cataclasites suggesting that these foliated cataclasites continued to develop after many of the oblique minor faults formed. Close to the foot (western side) of the outcrop

Fig. 2. Sketch of the Tsukide outcrop of the Median Tectonic Line fault contact, located in Fig. 1. The view is looking approximately horizontally (up to an inclination of 25° at the top) towards the East. The insert shows a close-up sketch of one of the sampling sites, with circles labelled 6a, 6b, etc. denoting sample positions in the fault zone. Arrowtails (crosses within circles) and arrowheads (points within circles) represent components of fault wall rock movement away from the viewer and towards the viewer, respectively. The stereograms are lower-hemisphere equal-area stereographic projections.

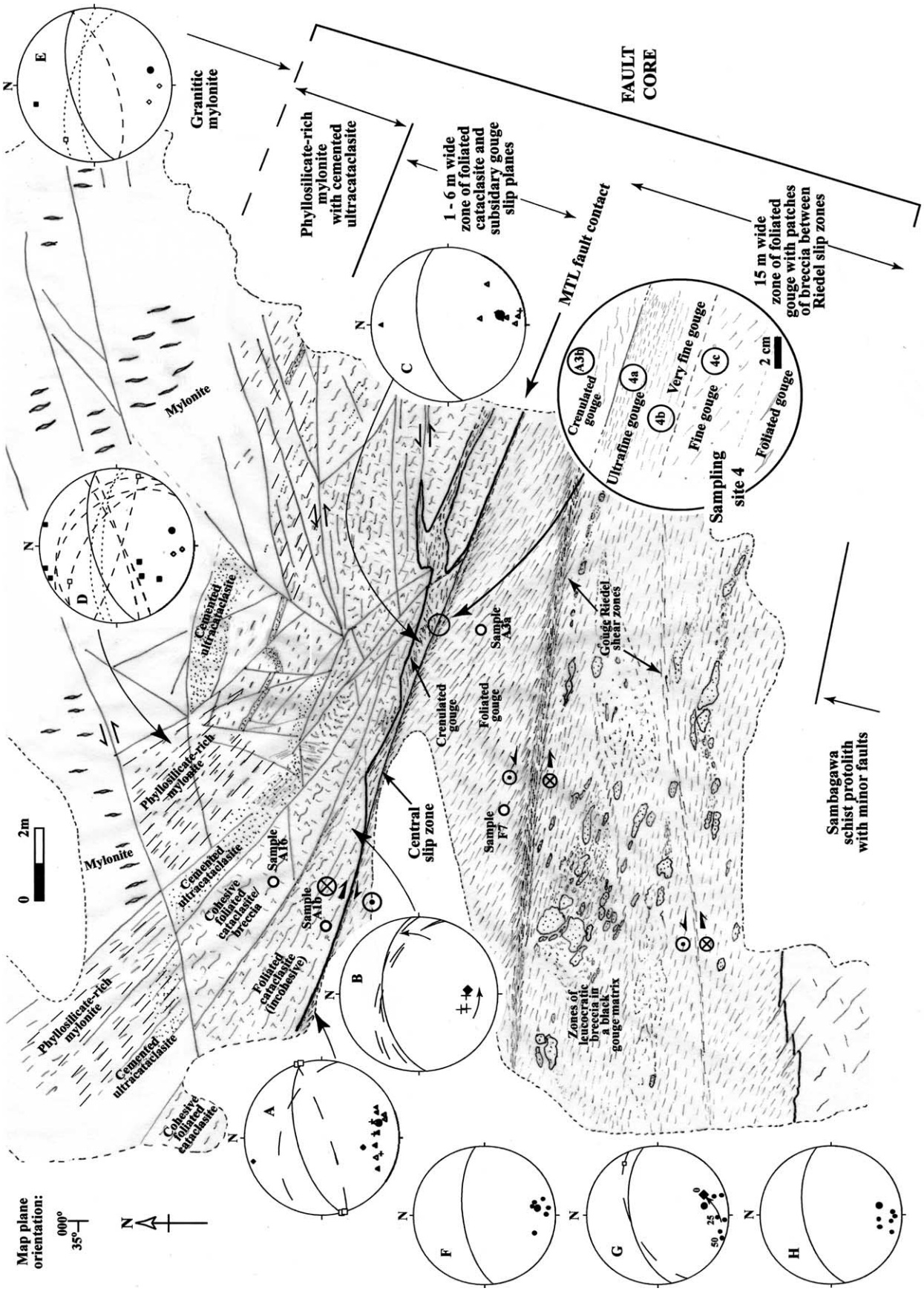
FAULT CORE
Granitic mylonite
Phyllosilicate-rich mylonite with cemented ultracataclasite
1 - 6 m wide zone of foliated cataclasite and subsidary gouge slip planes
MTL fault contact
15 m wide zone of foliated gouge with patches of breccia between Riedel slip zones
Mylonite
Cemented ultracataclasite
Phyllosilicate-rich mylonite
Cohesive foliated cataclasite/ breccia
Foliated cataclasite (incohesive)
Cohesive foliated cataclasite
Central slip zone
Crenulated gouge
Foliated gouge
Gouge Riedel shear zones
Zones of leucocratic breccia in a black gouge matrix
Sambagawa schist protolith with minor faults
Sample A3a
Sample A1b
Sample A1b
Sample F7
Sampling site 4
Crenulated gouge
Ultrafine gouge
Very fine gouge
Fine gouge
Foliated gouge
2 cm
0
2m
Map plane orientation:
000°
35°
N
A
B
C
D
E
F
G
H

around sampling site 6 (Fig. 2), interfingering and mixing has occurred between the coarse white gouge (derived from Ryoke fault rocks) and very fine black gouge adjacent to the Sambagawa foliated gouges. The interfingering is related to dextral R_1 Riedel slip surfaces of dextral shear sense in the foliated gouges on the south side of this contact, presumably formed during dextral reactivation. This suggests that the gouge mixing here was one of the most recent, shallowest deformation processes.

2.3. Microstructural data

The Ryoke mylonites contain feldspar porphyroclasts that are surrounded by aligned recrystallised quartz (termed 's-mylonites' in Takagi (1985)) and show patchy in situ alteration (Fig. 4a). Within the zone of variably fractured Ryoke mylonite, epidote with calcite and other carbonates and quartz-filled veins and ultracataclastic bands (Fig. 4b) suggest retrogression from Ca-rich feldspars in the mylonite. Close to the MTL fault contact, cataclasites show a wide variety of microstructures, varying in grain size, cementation and fabric. Cataclastic and ultracataclastic rocks often show evidence of multiple micro-brecciation/cement healing events, with some cemented areas themselves being deformed to gouge zones (Fig. 4c). Ryoke-derived white gouge and incohesive foliated cataclasites adjacent to the contact with the Sambagawa-derived fault rocks contain coarse quartz/calcite-cemented ultracataclasite microclasts within a foliated clayey matrix (Fig. 4d). In cohesive foliated cataclasites (Fig. 3), compositional banding of alternating quartz-rich and clay-rich gouge bands is commonly parallelled by cracks (Fig. 4e), some of which contain brown mineral fillings possibly from percolating surface-derived water.

Of the Sambagawa-derived gouges, the crenulated gouge within the localised intersection zone of a subsidiary fault and the main fault (close to sampling site 4; Fig. 3) contains a much higher proportion of opaque minerals than the other types (Fig. 4f). Microscale crenulations appear to have formed at the intersections of two different fabric orientations and contain calcite 'pressure shadow' tails on quartz clasts. This crenulated gouge does not occur elsewhere along the fault. The extremely fine gouge in the central slip zone contains an alignment fabric of clay flakes or aggregates of clay flakes (Fig. 4g). XRD data show a quartz + illite/muscovite matrix composition for the grain size fraction <0.6 μm. Quartz microclasts are present but these are much finer than for the other gouges (Fig. 5). The black Sambagawa-derived foliated gouge contains rounded microclasts of quartz/calcite-cemented ultracataclasite that often contain calcite-filled fractures (Fig. 4h). The fabric is defined both by elongate trails of microclasts, and by preferred orientation of grains in the phyllosilicate matrix. XRD data of foliated gouge samples suggest that they are composed of quartz, small amounts of Na-feldspar, with a matrix of chlorite and illite/muscovite. Samples of foliated gouge relatively close to the central slip zone show microstructures compatible with dextral shear, such as oblique shear bands (e.g. Fig. 4h). Given the sinistral kinematics of the larger scale Riedel shear zones in the foliated gouge (Fig. 3), this indicates the localised nature of deformation around the central slip zone during dextral reactivation on the MTL.

2.4. Grain size data

An important aspect of the MTL fault gouges described above is the variable proportion and size of microclasts present in the clay matrix. Microclast size distributions in the gouge were examined by particle sieving (minimum measurable size of 32 μm). Gouge samples taken from different positions within the MTL fault zone were oven dried, weighed, and then disaggregated. They were then mixed with distilled water to form a slurry which aided the washing through of fine clay aggregates at every sieving step. After each sieving step, the material of each size fraction was dried and weighed. The grain size data are presented in Fig. 5, showing that the Ryoke-derived white gouge is much coarser than the Sambagawa-derived gouges, and that the central slip zone gouges have the lowest proportions of microclasts. Samples within the foliated gouge collected further away from the central slip zone tend to have higher proportions of larger microclasts (Fig. 5).

2.5. Summary of fault zone structure

To summarise these observations of the structural nature of the MTL fault zone (Table 1), the widely differing lithologies on each side of the fault gave rise to a highly asymmetric fault zone structure. The *mylonites* in the Ryoke terrain (Zone A, Table 1) may be considered as protolith rocks to the brittle deformation along the MTL that generated a *variably fractured zone* (Zone B, Table 1) analogous to a heterogeneous damage zone (e.g. Chester and Logan,

Fig. 3. Outcrop map of the upper part of the Median Tectonic Line exposure in Fig. 2, showing the distribution of fault rock types and the central slip zone in the gouge. The close-up shows the sampling site at and around the central slip zone, with sample positions shown by the labelled circles. The stereograms are lower-hemisphere equal-area stereographic projections. Stereograms A and C represent fabrics at and around the central slip zone, B represents the foliated cataclasite, showing rotation of the foliation towards a subsidiary shear zone, D represents the phyllosilicate-rich mylonite, E represents the granitic Ryoke mylonite, and F, G and H represent the foliated gouge fabrics 0–50 cm, 50 cm–5 m, and 6.5–14 m from the central slip zone, respectively. The numbers in G denote the distance in centimetres from the centre of a Riedel shear zone. Key: large filled circle and bold great circle denote the central slip zone orientation, given in each stereogram for reference; filled diamonds and long dashed great circles—subsidiary shear zones; crosses—foliated cataclasite foliation; filled and open triangles—fabrics of the central gouge slip zone and surrounding gouge respectively; filled squares with short dashed great circles—fractures; small filled circles—foliated gouge foliation and open diamonds with dotted great circles—mylonitic foliation. Open squares represent lineations.

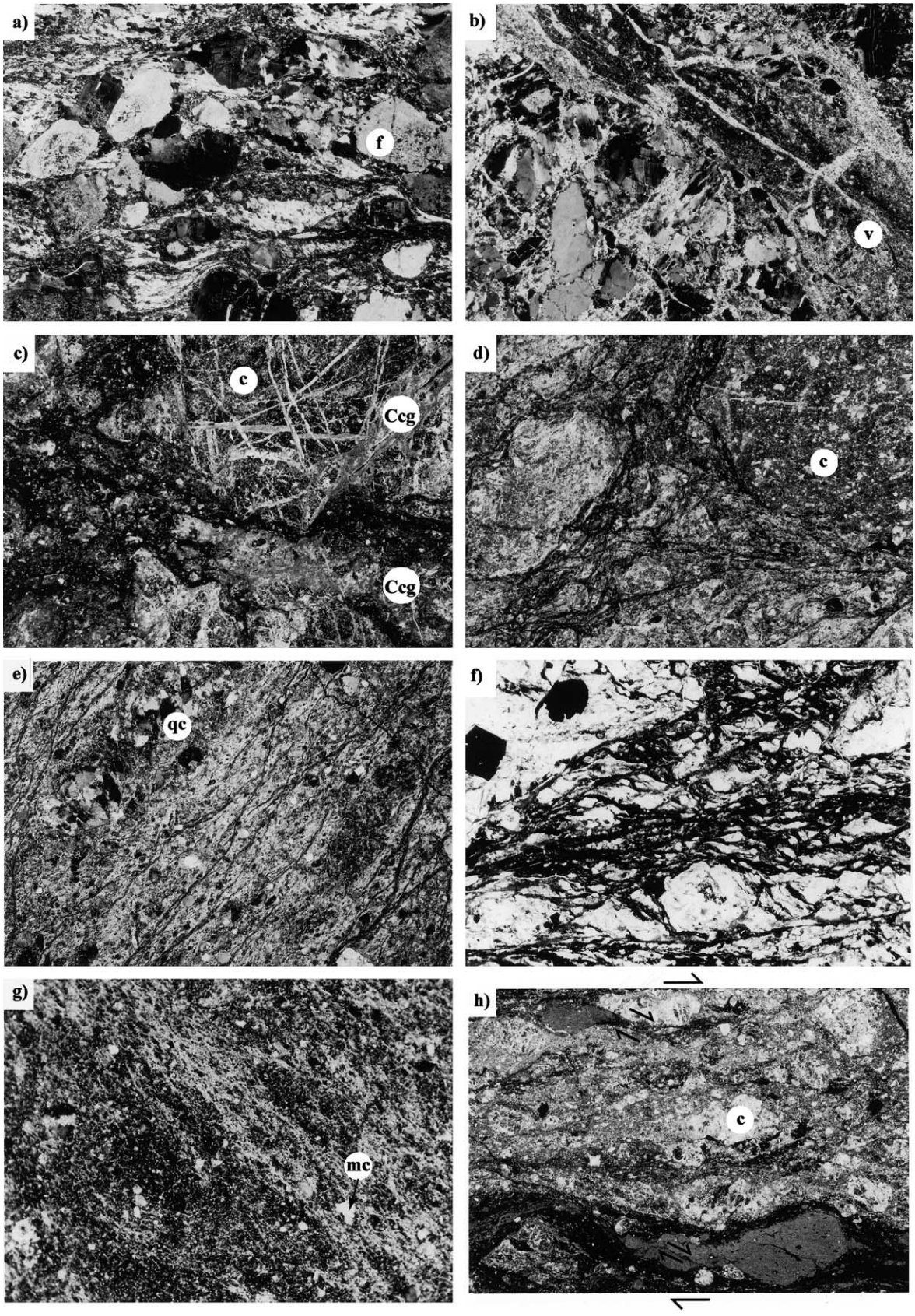
a)
f
b)
v
c)
c
Ccg
Ccg
d)
c
e)
qc
f)
g)
mc
h)
c

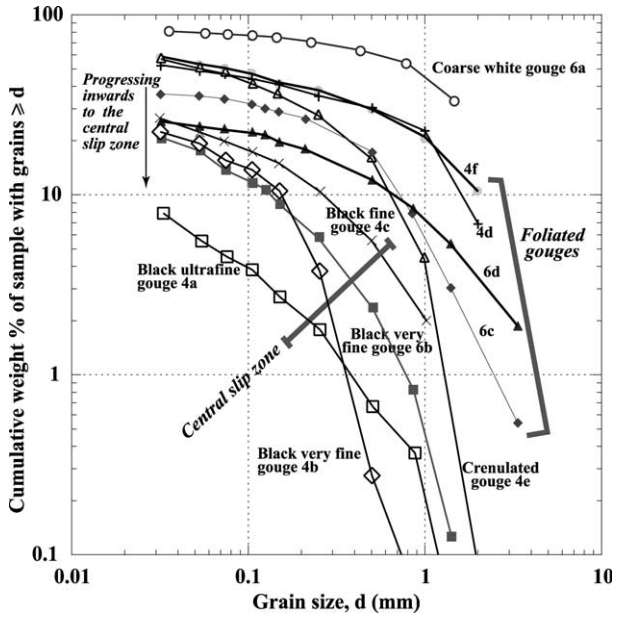

Fig. 5. The grain size distribution of microclasts of the different gouges from the Tsukide outcrop of the MTL. Note that the coarse grain size data is not concordant with the rest of the data, suggesting the under-sampling effect of the larger microclast sizes. The lower microclast grain size range is therefore more likely to be a general indicator of gouge microclast size.

1986; Evans et al., 1997) up to 300 m from the main MTL fault contact. Mineralisation and cementation is widespread in this zone, probably under lowest greenschist-grade conditions by analogy with other strike-slip fault zones (e.g. Anderson et al., 1983), with further cataclasis of cemented fault rocks also evidenced. *Phyllosilicate-rich mylonites* (Zone C, Table 1) up to 10 m from the fault contact, generated after initial fracturing of the feldspar, also have a significant brittle overprint. Localised cataclasis up to 4 m from the fault contact generated foliated *cataclasites* (cemented or incohesive) (Zone D, Table 1), within which white gouges close to the contact generated by comminution of cemented cataclasite remained coarse-grained and probably represented relatively shallow deformation (Anderson et al., 1983). On the other side of the fault contact, *metapelitic schist* (Zone G, Table 1) from the Sambagawa terrain does not show a damage zone, although some isolated minor faults were observed, along with minor fracturing at the contact with the fault zone. However, deformation of the Sambagawa schist by movement on the MTL appears to have been accommodated only in a 15-m-wide zone of *foliated gouge* (Zone F, Table 1). This gouge shows structures typical of localised strike-slip fault-related deformation in the top few kilometres of the Earth's crust. For example, low-angle synthetic (R_1) Riedel shears described in the field and from experiments (e.g. Tchalenko, 1968; Rutter et al., 1986; Logan et al., 1992), and a narrow fault-parallel *central slip zone* (Zone E, Table 1) are interpreted from mechanical data to represent gouge deformation stages of strain hardening/compaction and later stick-slip sliding, respectively (Logan et al., 1992). Such heterogeneously distributed deformation has previously been cited from strike-slip faults such as the Punchbowl fault in California (Chester and Logan, 1986) and the Carboneras fault in southeastern Spain (Rutter et al., 1986), and may be an important general feature. Furthermore, the planar central slip zone bounded by slickensides appears very similar to central slip zones in active faults examined after earthquakes, such as the Nojima and Neodani faults in southwestern and central Japan (e.g. Shimamoto et al., 2001 and references therein). Deformation mechanisms in the foliated gouge and this latest principal displacement zone are cataclastic grain size refinement with rotation of elongate grains, strain partitioning around clasts and localised micro-scale cataclastic flow generating fabrics, which suggest shear strain accommodation by bulk ductile flow. Progressive localisation of strain during continued deformation and exhumation is indicated by the increased grain size refinement towards the centre of the fault zone (Engelder, 1974; Anderson et al., 1983; Sammis et al., 1986). Alteration by water-induced retrogressive reactions generated clays in the centre of the fault zone at the expense of comminuted feldspar and chlorite. The resulting microstructure is probably a result of fragmentation of quartz and phyllosilicates, with accompanying compaction and syn-deformational precipitation of new phyllosilicates, similar to clay gouges described in other large strike-slip fault zones (e.g. Rutter et al., 1986).

Fig. 4. Optical photomicrographs of Median Tectonic Line fault rocks, taken under crossed-polars except where stated. (a) Relatively unfractured Ryoke granitic mylonite sample, taken 440 m North of the MTL. Feldspar porphyroclasts (f) show signs of post-deformation patchy internal alteration. Width of view is 3 mm. (b) Microfault zone (v), containing very fine-grained epidote and quartz, cross-cutting mylonitic foliation in brecciated Ryoke mylonite 160 m North of the MTL. Width of view is 3 mm. (c) Cemented ultracataclasite, taken from the Tsukide outcrop, 3 m North of the contact between Ryoke and Sambagawa-derived fault rocks. Clasts (c) of very fine-grained quartz mylonite are cut by narrow calcite veins, and larger calcite-rich gouge zones (Ccg). Width of view is 3 mm. (d) White gouge within foliated cataclasite from the Tsukide outcrop of the MTL, with clasts (c) of fine-grained quartz cut by thin calcite veins and surrounded by a clay-rich matrix whose fabric defines the foliation. Width of view is 12 mm. (e) Cohesive foliated cataclasite 0.5 m North of the contact between Ryoke and Sambagawa-derived fault rocks. Alternating coarser-grained and fine-grained layers define the foliation, with some zones of larger fractured quartz clasts (qc) still visible. Width of view is 12 mm. (f) Plane polarised light view of crenulated gouge 4 cm North of the central slip zone (Fig. 3) containing a high proportion of opaque material. The light areas are mostly reworked quartz cataclasite grains with some calcite fringes. Note the intersection of the two fabrics forming a crenulated appearance. Width of view is 3 mm. (g) Ultrafine gouge from the central slip zone at the Tsukide outcrop. Note the fabric of the aligned clay flakes and the smaller quartz microclasts (mc) than in the other gouges. Width of view is 1.2 mm. (h) Foliated black gouge, taken 5 cm South into the Sambagawa-derived gouges from the central slip zone. The Ryoke-derived clasts (c) of quartz ultramylonite and ultracataclasite are cut by calcite veins and surrounded by a clay-rich matrix. Width of view is 12 mm.

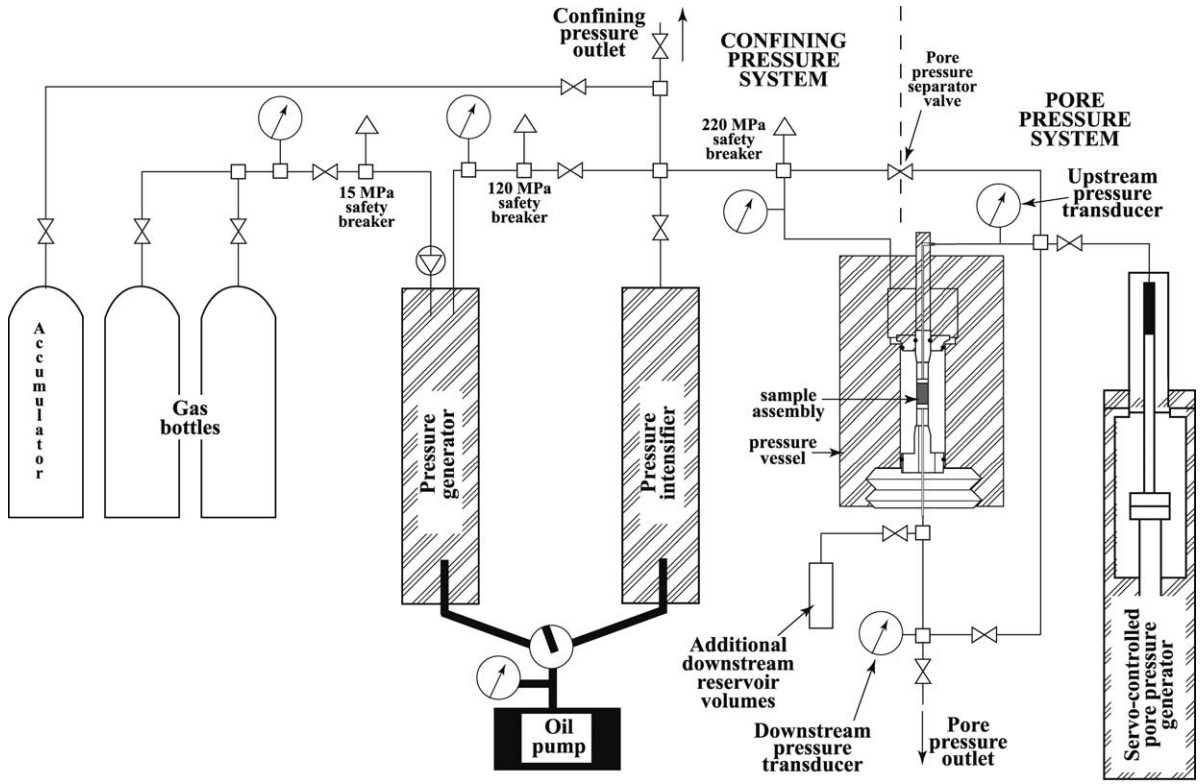

Fig. 6. Diagram of the high-temperature high-pressure deformation and fluid-flow gas apparatus at Kyoto University used to measure the permeabilities recorded in this paper.

3. Permeability measurements of Median Tectonic Line fault rocks

3.1. Experimental background

Permeability was measured using a high-temperature high-pressure deformation and fluid flow gas apparatus. The gas apparatus (Fig. 6) uses a pressure generator to apply confining pressures up to about 120 MPa, after which an intensifier may be used to achieve higher confining pressures. We are currently limited to 220 MPa by Japanese government regulation on the use of high-pressure gas equipment. The pressure vessel has an internal device to apply an axial force to the upper piston so the specimen is kept under uniform (isotropic) confining pressure. The vessel is placed in a servo-controlled dynamic loading frame with loading capability to 500 kN and dynamic response to 200 Hz. The pore pressure (P_p) system can be isolated from this and controlled separately by a fast-operating servo-controller, which enables P_p oscillation in the upstream reservoir with frequencies from 10^{-3} to about 10 Hz. The downstream reservoir volume can be adjusted to include larger volumes depending on the permeability range anticipated. In the experiments performed to date, both confining and pore pressures were applied using nitrogen gas as the pressure medium, at room temperature. The earlier experiments were undertaken at pressures up to 110 MPa for safety during testing of the system, after which a maximum confining pressure of 200 MPa was routinely used.

3.1.1. Sample preparation

The cylindrical samples of core used for permeability measurement were taken from the outcrops usually by means of inserting 20 mm internal diameter non-annealed copper tubes of 0.2 mm wall thickness into the outcrop and extracting them with the sample. Stainless steel tubes of 25 mm internal diameter, thinned to a wall thickness of around 0.5 mm, have also been used where the fault rock was too hard to use the copper tubes, especially in the coarser gouges. These cores were immediately transferred at the outcrop to polyolefin jackets using a specially designed portable piston-and-grip system, stoppered at the ends using porous sandstone plugs and heat-sealed in the jacket. For hard rocks such as the protoliths and cemented fault rocks, coring was done in the laboratory from blocks. The cores used mostly had lengths of between 10 and 40 mm (Table 2). All samples were cored parallel to foliation and lineation (where visible), except mylonite sample E25z and gouge sample 4a-z, which were perpendicular to foliation. The samples were oven dried at 80 °C for 2 days to eliminate pore water. Each of the samples was then placed between perforated brass spacers and further jacketed

Table 2
Summary of laboratory-derived permeability data for all the fault rocks in this study. * denotes data from the deconfining part of the confining pressure cycle

Fault rock zone	Fault rock type	Sample no.	Distance from MTL contact (m)	Sample length (mm)	Gas rig run no.	Permeability ($m^2 \times 10^{-18}$)				First confining step		Last confining step		First deconfining step		Last deconfining step	
						50 MPa	100 MPa	200 MPa	50* MPa	Pc step (MPa)	γ	Pc step (MPa)	γ	Pc step (MPa)	γ	Pc step (MPa)	γ
Ryoke mylonite	Granitic mylonite	E25-x	− 400	12.1	187	4.5	0.653	0.0258	0.0484	29.5 → 50	0.090	148 → 200	0.026	200 → 100	0.011	60 → 30	0.024
	Granitic mylonite	E25-z	− 400	18.0	151	1.92	0.193	0.034	0.749	30 → 50	0.070	148 → 200	0.018	200 → 70	0.014	70 → 30	0.07
Variably fractured mylonite	Cemented cataclasite	E17	− 245	31.0	143	701	23.1	1.44	18.9	31 → 41	0.091	160 → 200	0.021	200 → 160	0.000	40 → 30	0.130
	Artificially fractured cemented cataclasite	E17 refrac	− 245	31.0	144	8600	2660	501	1880	31 → 41	0.052	160 → 200	0.016	200 → 160	0.004	40 → 30	0.062
	Brecciated mylonite	E27	− 140	23.2	153	228	19	2.69	12.8	30 → 50	0.106	160 → 200	0.018	200 → 160	0.001	50 → 30	0.082
Cataclasites	Cemented foliated cataclasite	A16	− 2	26.7	142	235	0.367	0.00903	0.214	31 → 56	0.126	160 → 200	0.037	200 → 61	0.001	61 → 30	0.167
	Incohesive foliated cataclasite	A1b	− 0.1	32.3	150	1340	36.8	0.665	10.1	30 → 50	0.088	158 → 198	0.025	198 → 153	0.004	50 → 30	0.071
	Crenulated gouge	A3b	− 0.04	73.8	146	11700	3430	55.6	157	30 → 40	0.085	160 → 200	0.024	200 → 160	0.003	40 → 30	0.068
	Coarse white gouge	Cb	− 0.03	14.5	163	1100	28	0.94	3.44	31 → 50	0.119	160 → 200	0.034	200 → 160	0.002	50 → 30	0.070
	Coarse white gouge	6a	− 0.02	12.3	83	2075	55.58	–	32.1	31 → 50.5	0.136	90 → 109	0.057	109 → 90	0.0003	51 → 30	0.020
Central slip zone	Ultrafine gouge	4a-x	0.01	16.4	70	54	0.0806	0.00355	0.0263	30 → 53	0.199	169 → 201	0.012	201 → 141	0.007	95 → 30	0.042
	Ultrafine gouge	4a-z	0.01	11.1	261	48.6	0.00312	–	0.00759	30 → 50	0.225	174 → 201	–	201 → 149	–	51 → 30	0.0520
	Very fine gouge	4b	0.04	15.3	67	299	0.389	–	–	28 → 48	0.183	97 → 154	0.059	–	–	–	–
	Fine gouge	4c	0.08	29.0	84	163	0.3048	–	0.465	31 → 50.5	0.207	88.5 → 110	0.092	110 → 90	0.002	51 → 30	0.073
Sambagawa-derived foliated gouges	Foliated gouge	6c	0.1	13.6	87	134	4.19	–	3.82	30 → 50	0.130	90 → 110	0.052	110 → 90	0.003	50 → 30	0.034
	Foliated gouge	6d	0.2	28.4	90	55	1.536	–	1.48	30 → 50	0.148	90 → 110	0.057	109 → 90	− 0.005	50.5 → 30	0.047
	Foliated gouge	13E	0.8	12.7	27	20.83	3.07	–	2.74	28.5 → 49	0.097	90 → 109	0.044	109 → 90	0.002	50 → 30.5	0.022
	Foliated gouge	A3a	1.2	46.9	145	299	21.8	0.719	3.91	30 → 61	0.080	159 → 200	0.036	200 → 160	− 0.006	60 → 30	0.075
	Foliated gouge	F7a	4.5	23.7	317	4330	214	6.72	17.9	50 → 75	0.0636	174 → 200	0.0202	200 → 150	0.002	50 → 30	0.0526
Sambagawa schist	Metapelitic schist	D1	80	31.7	138	187	0.983	0.0211	0.726	29 → 60	0.126	149 → 202	0.040	202 → 112	0.008	60 → 30	0.118
Minor fault	Coarse gouge	5-1	200	12.0	88	549	48.5	–	42	30 → 50	0.101	90 → 110	0.031	110 → 90	− 0.006	50 → 30	0.024

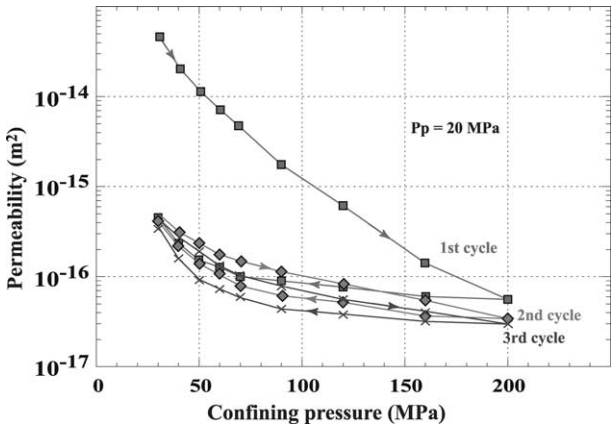

Fig. 7. Gas permeability data at a pore pressure of 20 MPa showing the effect of pressure cycling on sample A3b of foliated gouge.

with the upper and lower pistons using several layers of polyolefin to provide a 2–3-mm-thick layer of jacketing.

3.1.2. Permeability measurement methodology

Permeabilities were measured at a pore pressure (P_p) of 20 MPa using the sinusoidal pore pressure oscillation technique (Kranz et al., 1990; Fischer and Paterson, 1992) with a maximum amplitude of 1 MPa. Confining pressure was increased in steps from 30 MPa with permeability measurements at each step. Confining pressure was then decreased from a peak value with further permeability measurements along the way, to complete a set of measurements throughout a confining pressure cycle. We report our permeability data as a function of the confining pressure (P_c). Our data were obtained by monitoring the upstream and downstream

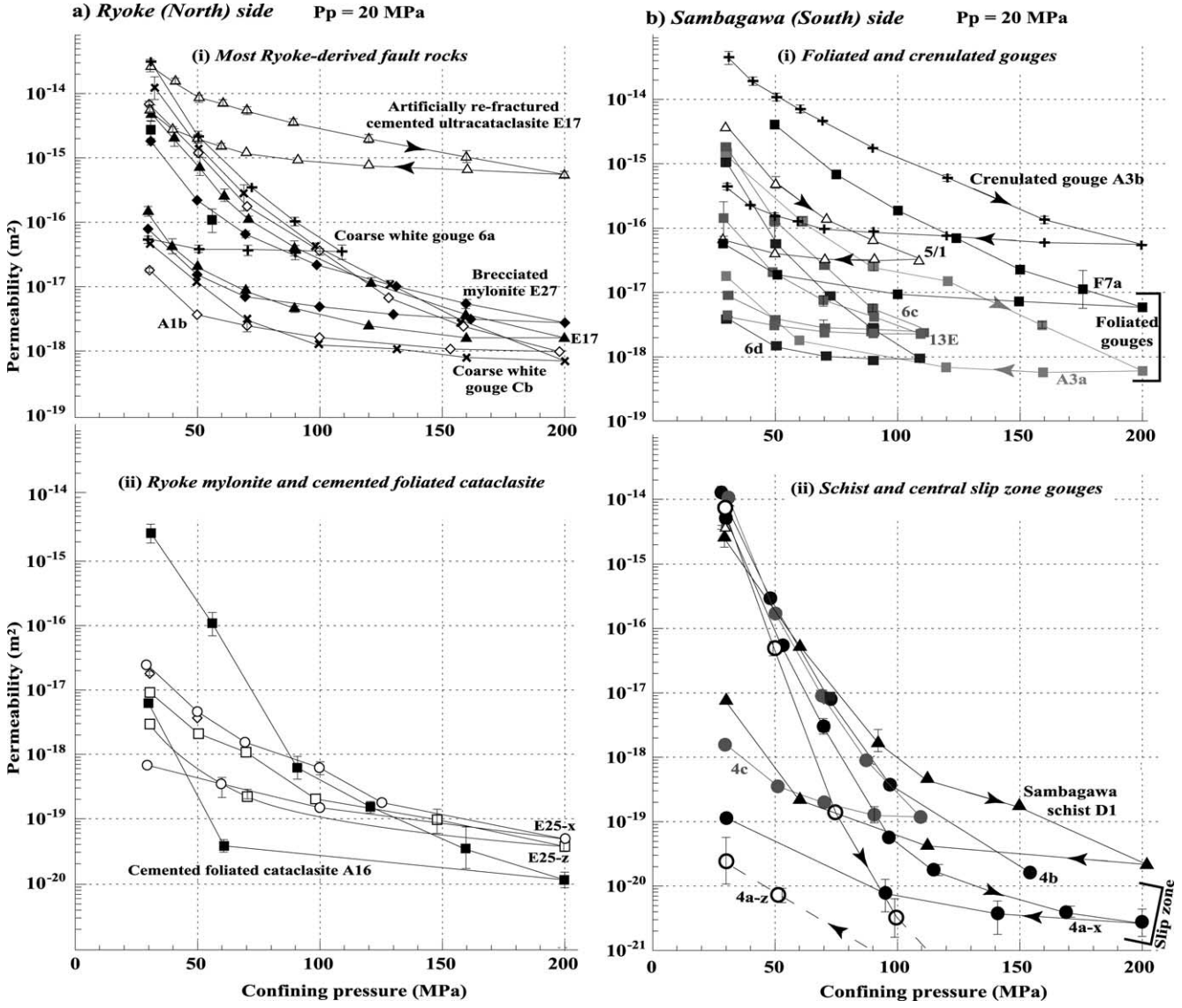

Fig. 8. Gas permeability data from the first pressure cycle for samples of MTL fault rocks and protoliths for a pore pressure of 20 MPa at room temperature (see Table 2 for summary). (a) Samples from the Ryoke (North) side: (i) all Ryoke-derived fault rocks except the cemented foliated cataclasite; and (ii) mylonite samples and cemented foliated cataclasite. (b) Samples from the Sambagawa (South) side: (i) foliated gouges, crenulated gouge and minor fault gouge; and (ii) central slip zone gouges and protolith Sambagawa schist. Error bars are only given where larger than the data symbol.

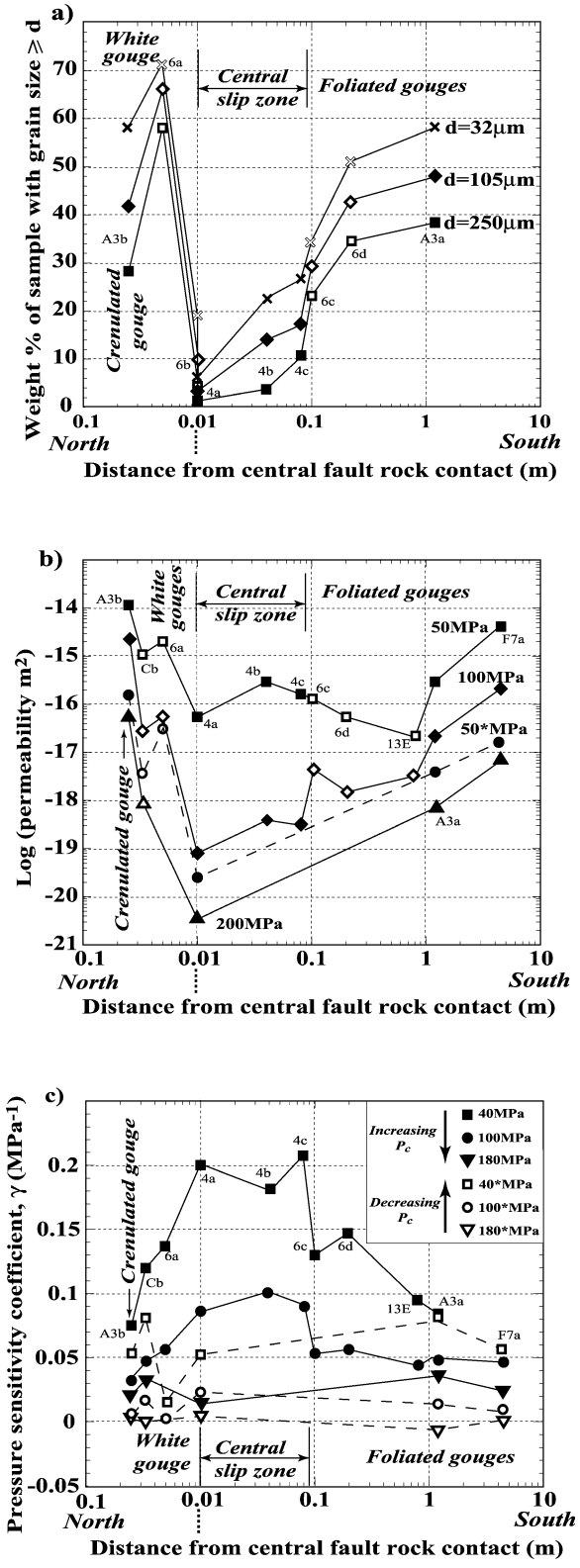

Fig. 9. Summary of the distribution of fault rock properties across the gouge zone of the MTL. (a) Microclast size proportions; (b) permeability at the confining pressures indicated, for a pore pressure of 20 MPa; (c) pressure sensitivity coefficient. * denotes the deconfining path. In (a) and (b) open symbols denote samples taken from a separate site to those of the closed symbols. In (c) closed symbols denote data from the confining path of the pressure cycle, and open symbols denote data from the deconfining path.

P_p oscillations using strain gauge pressure transducers, and enhancing the downstream output signal using a voltage shifter to optimise the voltage range that may be detected by the signal recorder for maximum sensitivity. The ratio of downstream-to-upstream P_p oscillation amplitudes and the phase lag were measured. From these two measured parameters, two dimensionless parameters were calculated using a numerical model based on equations given in Fischer (1992), from which permeability can be directly calculated. Permeability measurement error may be assessed for the P_p oscillation method either by estimating the uncertainties of the pressure transducers, and carrying these uncertainties through the calculations (e.g. Faulkner and Rutter, 2000), by performing systematic measurements at different oscillating frequencies, or by performing a detailed statistical treatment of repeated oscillation data. Error bars in this paper were calculated from statistical variance of repeated oscillation data and measurements across a range of oscillation frequencies.

3.2. Fault rock permeabilities

3.2.1. Permeability data and variation with pressure

In a typical pressure cycling experiment, permeability decreases markedly with increasing confining pressure (P_c) during the first pressure cycle (Fig. 7). Permeability does not fully recover during deconfinement in the first pressure cycle, and permeability at the end of the first cycle is typically two orders of magnitude or more lower than at the start (Fig. 7). During further pressure cycles, such permeability decreases continue to occur but are much smaller, and exhibit hysteresis. Data for each pressure cycle peak show a progressive decrease of permeability with further pressure cycling, though these decreases become smaller with every additional pressure cycle. Plotted on a logarithmic scale such as in Fig. 7, the permeability data during confinement for different cycles closely parallel one another after the first cycle. Furthermore the permeability data during the different deconfinement stages also parallel one another, including the first cycle data.

For the Ryoke mylonite-derived fault rocks (Fig. 8a; Table 2), samples fall into three classes of permeability data:

1. The lowest permeabilities were recorded in mylonites and cemented foliated cataclasites, in the order of 10^{-19} m^2 at a P_c of 100 MPa, and 10^{-20} m^2 at 200 MPa. However, at low confining pressures (around 30 MPa) the cemented foliated cataclasite showed a permeability two orders of magnitude higher than the mylonites.
2. The variably fractured mylonites and remaining cataclasites show higher permeabilities of around 10^{-17} m^2 at 100 MPa and 10^{-18} m^2 at 200 MPa.
3. Artificial fracturing of a sample of fractured cemented ultracataclasite (sample E17) was achieved by subjecting it to an axial stress of 100 MPa for 10 s. This generated

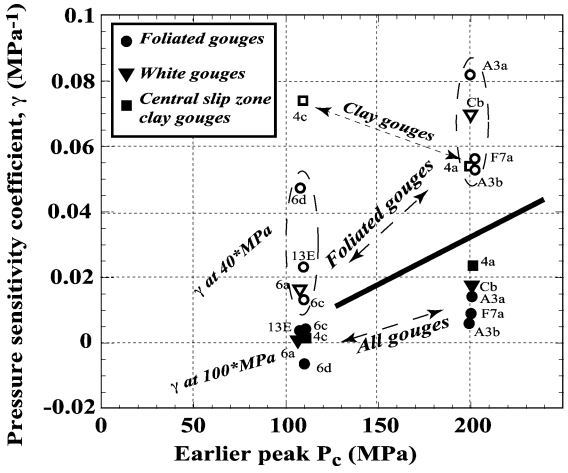

Fig. 10. The effect of previous effective pressure peak on later pressure sensitivity coefficients. Filled symbols denote coefficients at 100 MPa, and open symbols denote coefficients at 40 MPa, both on the deconfining path, for a pore pressure of 20 MPa.

new microcracks but no through-going failure surface. Later permeability measurements to demonstrate the effect of cement cracking yielded a permeability increase of up to two orders of magnitude, due probably to fracture dilatancy (e.g. Zoback and Byerlee, 1975a).

Permeability data for the Sambagawa-derived fault rocks and protolith do not show such a clear three-fold division (Fig. 8b). For simplicity of presentation, they have been divided into two groups:

1. The protolith Sambagawa schist and clay gouges of the central slip zone, which have low permeabilities.
2. The foliated gouges and crenulated gouge, which show higher permeabilities than the central slip zone gouge and protolith, albeit very variable.

The data show that at confining pressures of 100 MPa and greater, the central slip zone gouge has a permeability more than two orders of magnitude lower than the adjacent foliated gouges. Furthermore, the permeability is at least an order of magnitude lower for the sample taken perpendicular to the slip zone (sample 4a-z). Foliated gouges adjacent to this slip zone have much higher permeabilities (Table 2; Fig. 8b), that are between 0.5 and three orders of magnitude higher than for the Sambagawa schist protolith. A systematic decrease in gouge permeability (except for the 50 MPa data) occurs from the edge of the MTL fault zone into the central slip zone, in a similar pattern to the variation in gouge grain size with position within the fault zone (Figs. 5 and 9). A significantly higher permeability was measured in the crenulated gouge sample collected adjacent to the central slip zone on the north side (Fig. 3).

3.2.2. Pressure sensitivity coefficient of permeability

David et al. (1994) proposed a natural logarithmic law to describe permeability changes with pressure. For a relatively small confining pressure step of ΔP_c which causes a permeability change from k_1 to k_2, the permeability sensitivity to pressure can be described by a coefficient γ, where:

$$k_2 = k_1 \exp[-\gamma \Delta P_c]. \quad (1)$$

The pressure sensitivity coefficient, γ, is proportional to the gradient of the tangent of the data in Fig. 8 (the data in Fig. 8 is presented on a $\log_{10}$ graph, so the factor of proportionality is $-\mathrm{Ln}10$). Many of the data in Fig. 8 do not plot on straight lines described by a single gradient, so the definition of γ here is an approximation for small ΔP_c only. For the confining part of the pressure cycle, the data in Fig. 8b show that the central slip zone fault gouges have high γ at low pressures (around 0.2 MPa^{-1}), and the largest variability in γ with confining pressure, decreasing to around 0.012 MPa^{-1} at the 160–200 MPa interval. Typical maximum and minimum values of the cataclasites, foliated gouges and Sambagawa schist protolith are 0.12 and 0.04 MPa^{-1} at low and high pressures, respectively. However, the Ryoke mylonite and samples from the variably fractured mylonite zone have generally lower maximum and minimum values of around 0.09 and 0.02 MPa^{-1} at low and high pressures, respectively. The lowest γ values are always for the first small step on the deconfining portion of the pressure cycle (Table 2), and for most samples are extremely low or even negative (possibly due to increases in tortuosity as the sample undergoes anisotropic relaxation). γ always increases with further deconfinement, usually back to initial confinement values in the cohesive fault rocks but not in the incohesive ones.

4. Discussion

4.1. Variations in laboratory permeability measurements of MTL gouges

The fault gouge samples showed wide differences in both grain size distribution and permeability, in a systematic trend across the fault zone (Fig. 9). At high confining pressures (100–200 MPa), permeability increases with distance from the central slip zone ultrafine gouge by three orders of magnitude over 4 m. This systematic variation in permeability follows the changes in grain size data, with the exception of the localised lens of crenulated gouge (Fig. 3). Fig. 9a shows a strong tendency for the microclast size fractions to increase in proportion to the whole sample with increasing distance from the central slip zone. Microscopic examination of the gouges (Fig. 4) shows that the phyllosilicate matrix is composed of grains much finer than 32 μm, so the data in Fig. 9a correspond to a systematic increase in microclast size and/or proportion, with increasing distance from the centre of the fault zone. The likely increasing comminution of the microclasts in the foliated gouge closer to the slip zone, along with compaction and syn-deformational formation of new fine-grained clay, has resulted in a

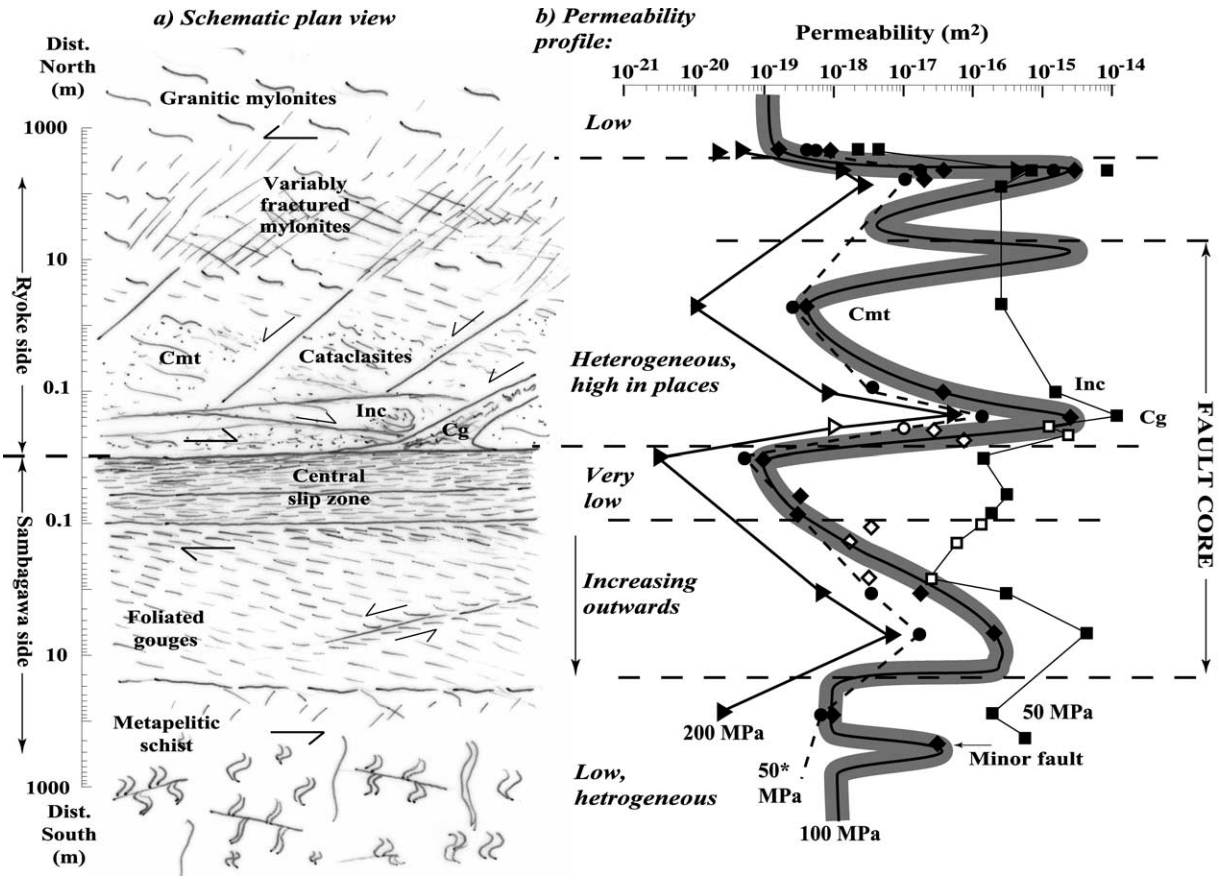

Fig. 11. Sketch summary of the main elements of permeability structure across the Median Tectonic Line. (a) Summary of the structural zones; (b) summary permeability data distribution for different confining pressures (stated at the base, with * denoting data from the deconfining path), for 20 MPa pore pressure, given the mapped distribution of fault rocks shown in Figs. 1–3. Note that the distance axis is logarithmic in both directions away from the Ryoke/Sambagawa contact. 'Cmt' and 'Inc' denote cemented and incohesive foliated cataclasites, respectively, and 'Cg' denotes crenulated gouge.

systematically decreasing permeability with increasing deformation localisation.

At low pressures such as 50 MPa, however, the contribution of microcracks and foliation partings to the overall fluid pathway is likely to be high. Fine gouges with few larger microclasts may contain better connected microcracks and foliation partings parallel to their better developed gouge fabrics, resulting in higher permeabilities than other gouges at low pressures. The onset of a strong positive correlation between permeability and grain size may suggest the limit of effect of such sample (artificial or natural damage) cracks on permeability.

4.2. Variations with pressure and implications for compaction mechanisms

Some previous works have suggested that a negative exponential relationship (constant pressure sensitivity coefficient, γ) holds between permeability and effective pressure during pressure increase. This relationship appears to be a good approximation to data on sandstones (David et al., 1994) and from various fault rocks (Evans et al., 1997; Seront et al., 1998), but does not hold for most of the data in this study (Fig. 8). For MTL gouges, the variation in sensitivity is reduced by pressure cycling, but additional ongoing experiments show that this can continue even until the tenth cycle. This is probably because we are able to use a wider range in effective pressures, allowing a greater range in compaction mechanisms (including repair of sample damage) to impact on the data. Data for the first cycle (Fig. 9c) show large variations in pressure sensitivity coefficient across the gouge zone at low pressures during confinement (P_c increase), but consistently low values at high P_c (during the P_c step 160–200 MPa). During confinement at low pressures, the finer-grained gouges show much larger pressure sensitivity coefficients than coarser gouges, presumably due to matrix compaction operating more efficiently in the finer gouges than in the coarse gouges where a microclast-supporting framework can protect the fine-grained matrix.

The permeability data in Fig. 8 show similar pressure sensitivities in the low pressure regions of the deconfining (decreasing P_c), and confining parts of the curves (e.g. sample A16). This suggests the operation of an elastic compaction/decompaction mechanism in this pressure interval. Previous work (David et al., 1994) proposed that

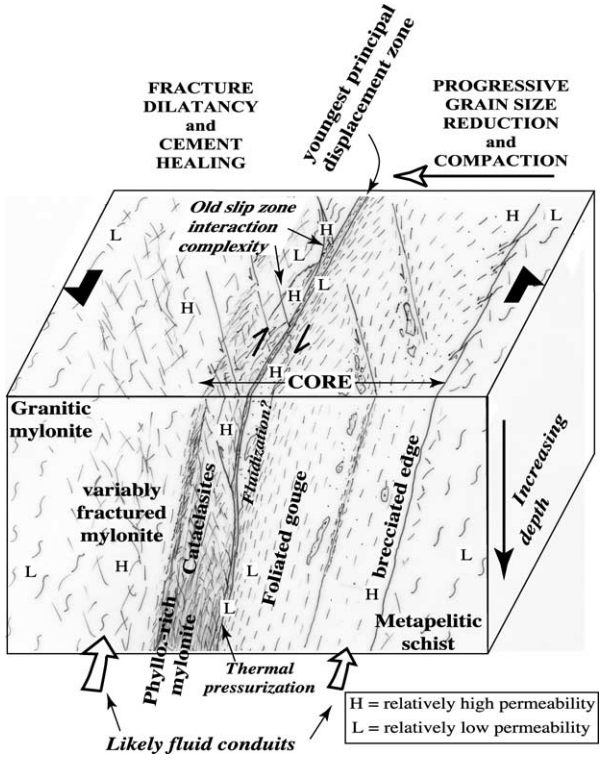

Fig. 12. Summary model of fluid flow behaviour in the shallow crust in and around the Median Tectonic Line fault zone. Note that the central portion is exaggerated in scale.

similarly high γ values are probably due to crack closure, and may include foliation-parallel partings in the foliated MTL fault rocks. The pressure at which γ decreases may therefore represent the limit to which closure of such cracks is dominant as a compaction and permeability-reducing mechanism. The gouges do not show such recovery upon deconfinement, suggesting that permeability decrease during initial confinement permanently repaired sample damage.

The effect on permeability of a change in pore pressure is not necessarily identical to that of an equal and opposite change in confining pressure. In other words, for an effective pressure P_e:

$$P_e = P_c - \alpha P_p \quad (2)$$

where the factor α is reported to be typically one or less (e.g. Bernabé, 1987), depending on the geometry and connectivity of pores and tortuosity. We have not measured permeability at different pore pressures, but may couple our textural and permeability data with findings in previous works to infer likely α for different fault rocks (see also Evans et al., 1997). In crystalline rocks, isolated microcrack dilatancy may lead to $\alpha < 1$, but will probably approach $\alpha = 1$ as fracture connectivity improves (Walsh, 1981) such as in the variably fractured mylonites. In phyllosilicate/quartz gouge mixtures, high matrix compressibility could be greater than that of the quartz clast framework leading to $\alpha > 1$ where both of these components are important in the rock microfabric (Zoback and Byerlee, 1975b). However, as comminution and breakdown of the framework proceeds in the gouge phyllosilicate matrix properties will dominate, leading to a single component behaviour and $\alpha \sim 1$ in the fine-grained centre of the fault zone. These suggestions remain to be tested by experiments at different pore pressures.

The previous highest effective pressure can be important in controlling future permeability at lower effective pressures in at least two ways. Firstly, at any given pressure on the deconfining path, the higher the previous peak $P_c - P_p$, the lower the measured permeability. Examples of this are in Fig. 8a by comparing data from adjacent coarse white gouge samples 6a (peak $P_c - P_p = 110$ MPa) and Cb (peak $P_c - P_p = 180$ MPa), and this effect has also been shown by Bolton et al. (1998) and Zhang and Cox (2000). Secondly, the pressure sensitivity of permeability during deconfinement also depends on by what proportion $P_c - P_p$ has dropped from its peak value. Fig. 10 shows that both at 100 and 40 MPa on the deconfining pathway, gouge pressure sensitivity values are higher for those samples subjected to peak $P_c - P_p$ of around 200 MPa than those samples subjected to peak $P_c - P_p$ of 110 MPa. The control of previous peak $P_c - P_p$ on pressure sensitivity of permeability must therefore be taken into account in modelling fluid pressure build-up in fault zones.

4.3. Significance for models of fault zone permeability structure in the upper crust

4.3.1. Relevance of laboratory results to in situ flow models in the crust

The Tsukide outcrop of the MTL was excavated by a local government project to a depth of 2–4 m before we started our work, so our fault rock samples are therefore relatively fresh and free from the effects that surface biochemical weathering processes may have had on the microstructure and consequent permeability measurements. Other laboratory permeability studies on fault gouge collected at freshly excavated outcrops, such as the Nojima fault (Mizoguchi et al., 2000) show no significant difference with analogous core data from nearby boreholes through the same gouge zone (Lockner et al., 1999). Many of the cohesive fault rocks are highly fractured, allowing the influx of surface-derived waters that may precipitate material within and form crack 'bridges', which may cause a higher permeability and lower pressure sensitivity of permeability (Morrow and Lockner, 1994). Such precipitates are only evidenced in cemented foliated cataclasites (Fig. 4e) that yielded low permeability at high pressure despite the possible presence of surficial crack fillings. Measurements of permeability of phyllosilicate-rich fault gouges using both gas and water show that water permeability tends to be lower by up to one order of magnitude (Faulkner and Rutter, 2000). The Klinkenberg effect may additionally cause a higher measured gas permeability than true permeability.

Following the simple treatment of this problem by Faulkner and Rutter (2000) (their Eq. 2), this overestimation was calculated to be about 10% at maximum.

The scale problem of using laboratory cores to infer larger scale permeability structure must also be considered (e.g. Coyle and Zoback, 1988). Permeability measurements during laboratory experiments of fracture dilatancy (Zoback and Byerlee, 1975a) yielded diffusion coefficients a few orders of magnitude lower than those calculated by the analysis of field data on flow around earthquake focal regions. This suggests that, for the case of significant deviatoric stress, fluid flow in laboratory core-scale microcracks is not representative of large-scale flow in fractures and joints which we cannot easily sample in laboratory core work. However, in situ permeability data for crystalline rocks, probably fractured, range between 10^{-13} and 10^{-18} m^2 for depths of up to 2 km (e.g. Brace, 1984). Furthermore, recent water injection experiments around the Nojima fault, at low deviatoric stress after a large earthquake, give in situ permeability estimates of 10^{-14}–10^{-15} m^2 (Tadokoro et al., 2001). Laboratory permeability data for the fractured rocks and cataclasites from the MTL (Fig. 8a) fall within these values at low pressures except for the cemented sample A16, albeit in a narrower range. Such a scale problem may therefore not be as significant (except for relatively wide natural fractures) for the case of isotropic stress as it would be for the case of significant deviatoric stress (e.g. Brown and Bruhn, 1998).

4.3.2. Summary of MTL permeability structure and comparison with previous models

A summary of the integrated structure and laboratory permeability data (Fig. 11) divides the MTL into five zones:

1. Relatively unfractured Ryoke mylonites of low permeability.
2. Variably fractured mylonites and cataclasites of very heterogeneous permeability—permeability is high in the fractured/veined rocks, and also in incohesive cataclasites, whereas it is low in cemented fault rocks that have not been refractured.
3. A narrow central slip zone of extremely fine-grained fault gouge of very low permeability, considered to be the most recent principal displacement zone.
4. A 15-m-wide zone of foliated gouge whose foliation-parallel permeability increases steadily as grain size increases from the central zone towards the edge of the fault zone.
5. Metapelitic Sambagawa schist of moderately low permeability, locally increased in isolated minor fault zones even a few hundred metres away.

Our laboratory permeability data at room temperature on these fault rocks exhumed to the surface is probably only applicable to fault permeability models in the upper crust (Fig. 12). Hence we consider the Ryoke mylonite and Sambagawa schist rocks as the two protoliths to low temperature deformation events focused on the MTL. The relatively low permeability of Ryoke mylonite protolith has become enhanced in a zone up to 300 m North of the MTL by *fracture damage and brecciation* in a zone of cataclastic overprinting of the mylonitic fabrics. Furthermore, alteration of the mylonite and mineralisation in the breccias and fracture network suggest that the fractured zone served as a conduit for fluid flow in the past, and is comparable with the damage zones of permeability enhancement described in previous, relatively simple models for fault zone permeability structure (e.g. Caine et al., 1996; Evans et al., 1997). Similar work on comparable mineralised fracture zones around faults suggest that such fracturing and fluid flow are episodic and related to earthquake deformation (Sibson, 1986; Bruhn et al., 1994). Coupled deformation and permeability experiments in progress on MTL fault rocks (Uehara, pers. comm., 2001) show that permeability in cemented cataclasites is enhanced by fracture dilatancy. The inter-relationship between *fracture dilatancy* and *cementation* is suggested to control permeability structure in the Ryoke mylonite-derived portion of the fault zone.

Fracturing and cataclasis of Sambagawa schist also resulted in enhanced permeability, as evidenced by the high permeability of foliated gouges adjacent to the Sambagawa schist protolith. Finer grain sizes and increased proportions of platey grains increase the efficiency of grain packing, resulting in shear-enhanced compaction and permeability decrease (e.g. Mandl et al., 1977; Teufel, 1987; Zhu and Wong, 1997) during continued, localised, deformation of the foliated gouge (Fig. 12). This zone cannot, therefore, be viewed in terms of the simple damage zone/fault core model of permeability structure (Caine et al., 1996) despite the high outer permeability, in contrast with the Ryoke mylonite-derived portion of the fault. This illustrates the importance of protolith lithology and mechanical properties for the type of structures developed in and around the fault zone (see also Schulz and Evans, 2000) and consequent permeability structure (Chester and Logan, 1986; Seront et al., 1998). The interplay between *cataclasis, shear-enhanced compaction* and *clay formation* has controlled the permeability structure in the metapelitic schist-derived portion of the fault zone and, coupled with localisation of deformation, has resulted in a very low permeability central slip zone. The low permeability central slip zone is surrounded by other highly deformed fault rocks in a complex spatial distribution across a 25-m-wide zone (Figs. 2 and 3), all of which would normally be considered the structural core of the MTL fault zone (Fig. 11). Hence, even within the highly deformed central portion of the MTL fault zone, permeability is highly variable and depends upon microstructure and degree of cementation in contrast with the previous basic model of Caine et al. (1996).

4.3.3. Implications for the mechanics of earthquake slip propagation

The very low permeability of the central slip zone suggests that frictionally heated pore fluids during a rapid slip event may undergo pressurisation rather than be allowed to flow out into surrounding higher permeability rocks in the fault zone. This increase in fluid pressure could cause dynamic weakening by resulting in an effective normal stress decrease, resulting in a large coseismic stress drop (Sibson, 1973). The rate of fluid escape out of the deforming low permeability zone is a crucial factor in governing this process. The likelihood of this thermal pressurisation process occurring therefore depends very much on the relative rates of propagation of the thermal and fluid pressure waves (Lachenbruch, 1980; Mase and Smith, 1987), requiring a smaller hydraulic diffusivity (a_h) than thermal diffusivity (a_t). The necessary permeability condition for this is derived by rewriting this inequality $a_h < a_t$ in terms of permeability, k (following definitions in Mase and Smith (1987)), to obtain:

$$k < \frac{K_{sf}\beta\mu_w}{(\rho c)_{sf}} \tag{3}$$

where μ_w is the dynamic viscosity of water (for which we use a value of 3.3×10^{-4} Pa s appropriate to 100 °C), β is the bulk compressibility of the fault rock, and K_{sf} and $(\rho c)_{sf}$ are the thermal conductivity and density × specific heat capacity of the solid–fluid composite, respectively. β has contributions from pore water, solid grain and composite compressibilities, very much depending on porosity and pore compressibility for which ongoing measurements are obtaining suitable data. Following Mase and Smith (1987) we assume $K_{sf} = 2$ W m^{-1} K^{-1} and $(\rho c)_{sf} = 2.6 \times 10^6$ Kg m^{-1} s^{-2}, and use an initial estimate of $\beta = 1 \times 10^{-10}$ Pa^{-1}. Using these values in Eq. (3) suggests that the condition $a_h < a_t$ is satisfied when $k < 2.5 \times 10^{-20}$ m^2. Permeability data of gouges from the central slip zone (Fig. 8) give similarly low values provided $P_c - P_p$ has been increased to at least 60 and 120 MPa for flow perpendicular and parallel to the fabric, respectively. This initial analysis suggests that principal displacement zone permeabilities are low enough for such a process to be important in reality provided that the gouge had previously been subjected to an effective mean stress above these values.

The presence of many oblique minor faults close to the principal displacement zone suggests that previous fault ruptures had occurred through many different fault rocks within the central core portion of the fault zone. Rates of pore pressure changes in slip zones during earthquakes have been demonstrated in models (e.g. Miller, 2002) to control stresses around rupture propagation fronts and the amount of stress drop. Such rates of pore pressure change depend on fault rock permeability and we have shown this to be highly variable, even over the centimetre to metre scale. Hydromechanically-controlled characteristics of earthquake slip such as thermal pressurisation will therefore depend on which part of the fault zone the slip event propagates through (Fig. 12), and could make pore pressure recharge times (and possibly interseismic times) very unpredictable.

4.3.4. Summary

In summary, the general hydrological behaviour of the MTL in the shallow crust may in part be similar to the simple model of Caine et al. (1996), but the structural core of the fault is more complicated. High permeability variations and the degree of continuity and connectivity of the low and high permeability zones in the fault core (Section 2.2.2) must be taken into account, all of which have an important bearing on models of rupture propagation and strength evolution. Outcrop observations suggest that most of the structural complexity of the fault zone was generated during the main sinistral shear along the MTL, so that the permeability structure of the fault zone was already complex prior to reactivation. Deformation associated with dextral reactivation is localised in the centre of the fault core, at and around the contact between the Ryoke-derived and the Sambagawa-derived fault rocks. This suggests that the youngest (shallowest) fault rocks are the weakest, and that the contact could have acted as a rheological boundary to focus deformation. The structural core of the MTL is more complex than described for other large strike-slip faults (e.g. Chester et al., 1993) despite evidence for deformation localisation and weakening, yet as in other cases the most recent principal displacement zone best maintains structural continuity along the fault (Fig. 12).

5. Conclusions

Combined structure and permeability data from the MTL show an asymmetric permeability structure in contrast to previous models:

1. On the north side of the fault zone, a variably fractured mylonite zone and cataclasites localised close to the fault contact have highly heterogeneous permeability structure, controlled by degree of fracturing, mineralisation and re-fracturing of cemented fault rocks.
2. On the south side of the fault zone, metapelitic schist suffered fracturing and comminution to produce a foliated gouge. Deformation in the gouge progressively localised towards the centre of the fault zone, resulting in increased comminution and metamorphic generation of clays that lead to a systematic decrease in permeability moving inwards to the centre of the fault zone.
3. Fault zone permeability structure is controlled by the interplay between fracture dilatancy, cementation, shear-enhanced compaction and clay formation. The importance of each of these processes depends very much on protolith lithology and low-grade metamorphic reactions.

A well-defined central slip zone of extremely fine gouge appears to have accommodated the most recent seismic slip events, and has the lowest permeability of all the fault rocks measured. For the gouges in general:

1. A good correlation exists for certain pressures between permeability and microclast size distribution in the gouge that may lead to a predictable tool for the permeability of a fixed gouge composition.
2. Both permeability and pressure sensitivity coefficient during deconfinement depend upon the earlier peak $P_c - P_p$ value, and relatively high fluid pressures would be required to significantly increase permeability in the central slip zone.
3. An initial analysis suggests that principal displacement zone permeabilities are low enough for thermal pressurisation to be an important dynamic weakening process provided that the gouge had previously been subjected to an effective mean stress in the range 60–120 MPa.

The Median Tectonic Line has a long-lived history of progressive strike-slip deformation during exhumation generating fault rocks at a variety of conditions. The range and complexity of structural processes affecting fault rock generation and microstructure, and therefore permeability structure, may consequently be larger than for other faults. Within the central 'core' zone, lateral continuity is best for the youngest fault rocks in the centre. Geological evidence suggests these fault rocks are the weakest, suggesting weakening in the MTL fault zone with continued deformation and/or exhumation. Their continuity means they have an important impact on hydro-mechanical properties of the fault during earthquake slip.

Acknowledgements

The first author acknowledges the support of a Science and Technology Fellowship from the European Commission. We thank Kanetaka Suwa and Hideo Takagi for introducing us to the spectacular outcrop at Tsukide, which motivated this study, and the latter also thanked for feedback on fabric chronology data. Discussion with Shinichi Uehara, Kazuo Mizoguchi and Takehiro Hirose helped in sampling and undertaking the laboratory measurements. Thorough reviews from Dan Faulkner and David Gray, and the editorial guidance of Jim Evans helped greatly to improve the manuscript.

References

Anderson, J.L., Osborne, R.H., Palmer, D.F., 1983. Cataclastic rocks of the San Gabriel fault—an expression of deformation at deeper crustal levels in the San Andreas fault zone. Tectonophysics 98, 209–251.

Bernabé, Y., 1987. The effective pressure law for permeability during pore pressure and confining pressure cycling of several crystalline rocks. Journal of Geophysical Research 92, 649–657.

Bolton, A.J., Maltman, A., Clennell, M.B., 1998. The importance of overpressure timing and permeability evolution in fine-grained sediments undergoing shear. Journal of Structural Geology 20, 1013–1022.

Brace, W.F., 1984. Permeability of crystalline rocks: new in situ measurements. Journal of Geophysical Research 89, 4327–4330.

Brown, S.R., Bruhn, R.L., 1998. Fluid permeability of deformable fracture networks. Journal of Geophysical Research 103, 2489–2500.

Bruhn, R.L., Parry, W.T., Yonkee, W.A., Thompson, T., 1994. Fracturing and hydrothermal alteration in normal fault zones. Pure and Applied Geophysics 142, 609–644.

Byerlee, J., 1990. Friction, overpressure and fault normal compression. Geophysical Research Letters 17, 2109–2112.

Caine, J.S., Evans, J.P., Forster, C.B., 1996. Fault zone architecture and permeability structure. Geology 24, 1025–1028.

Chester, F.M., Logan, J.M., 1986. Implications for mechanical properties of brittle faults from observations of the Punchbowl fault zone, California. Pure and Applied Geophysics 124, 77–106.

Chester, F.M., Chester, J.S., 1998. Ultracataclasite structure and friction processes of the Punchbowl fault, San Andreas system, California. Tectonophysics 295, 199–221.

Chester, F.M., Evans, J.P., Biegel, R.L., 1993. Internal structure and weakening mechanisms of the San Andreas Fault. Journal of Geophysical Research 98, 771–786.

Chu, C.L., Wang, C.Y., Lin, W., 1981. Permeability and frictional properties of San Andreas fault gouges. Geophysical Research Letters 8, 565–568.

Coyle, B.J., Zoback, M.D., 1988. In situ permeability and fluid pressure measurements at approximately 2 km depth in the Cajon Pass research well. Geophysical Research Letters 15, 1029–1032.

David, C., Wong, T.-F., Zhu, W., Zhang, J., 1994. Laboratory measurement of compaction-induced permeability change in porous rocks: implications for the generation and maintenance of pore pressure excess in the crust. Pure and Applied Geophysics 143, 425–456.

Engelder, J.T., 1974. Cataclasis and the generation of fault gouge. Bulletin of the Geological Society of America 85, 1515–1522.

Etheridge, M.A., Wall, V.J., Vernon, R.H., 1983. The role of the fluid phase during regional metamorphism and deformation. Journal of Metamorphic Geology 1, 205–226.

Evans, J.P., Forster, C.B., Goddard, J.V., 1997. Permeability of fault-related rocks, and implications for hydraulic structure of fault zones. Journal of Structural Geology 19, 1393–1404.

Faulkner, D.R., Rutter, E.H., 1998. The gas-permeability of clay-bearing fault gouge at 20 °C. In: Knipe, R.J., Jones, G., Fischer, Q. (Eds.), Faulting, Fault Sealing and Fluid-flow in Hydrocarbon Reservoirs. Geological Society Special Publication 147, pp. 147–156.

Faulkner, D.R., Rutter, E.H., 2000. Comparisons of water and argon permeability in natural clay-bearing fault gouge under high pressure at 20 °C. Journal of Geophysical Research 105, 16415–16426.

Fischer, G.J., 1992. The determination of permeability and storage capacity: pore pressure oscillation method. In: Evans, B., Wong, T.-F. (Eds.). Fault Mechanics and Transport Properties of Rocks. Academic Press, London, pp. 187–211.

Fischer, G.J., Paterson, M.S., 1992. Measurement of permeability and storage capacity in rocks during deformation at high temperature and pressure. In: Evans, B., Wong, T.-F. (Eds.). Fault Mechanics and Transport Properties of Rocks. Academic Press, London, pp. 213–252.

Fyfe, W.S., Price, N.J., Thompson, A.B., 1978. Fluids in the Earth's Crust. Elsevier, Amsterdam.

Hara, I., Shyoji, K., Sakurai, Y., Yokoyama, S., Hide, K., 1980. Origin of the Median Tectonic Line and its initial shape. Memoirs of the Geological Society of Japan 18, 27–49.

Hickman, S., Sibson, R., Bruhn, R., 1995. Introduction to special section: Mechanical involvement of fluids in faulting. Journal of Geophysical Research 100, 12831–12840.

Ichikawa, K., 1980. Geohistory of the Median Tectonic Line of Southwest Japan. Memoir of the Geological Society of Japan 18, 187–212.

Kerrich, R., 1986. Fluid infiltration into fault zones: chemical, isotopic, and mechanical effects. Pure and Applied Geophysics 124, 225–268.

King, C.-Y., Azuma, S., Igarashi, G., Ohno, M., Saito, H., Wakita, H., 1999. Earthquake-related water level changes at 16 closely clustered wells in Tono, central Japan. Journal of Geophysical Research 104, 13073–13082.

Kranz, R.L., Saltzman, J.S., Blacic, J.D., 1990. Hydraulic diffusivity measurements on laboratory rock samples using an oscillating pore pressure method. International Journal of Rock Mechanics, Mining Sciences and Geomechanics Abstracts 27, 345–352.

Lachenbruch, A., 1980. Frictional heating, fluid pressure, and the resistance to fault motion. Journal of Geophysical Research 85, 6097–6112.

Lockner, D., Naka, H., Tanaka, H., Ito, H., Ikeda, R., 1999. Permeability and strength of the Nojima core samples from the Nojima fault of the 1995 Kobe earthquake. In: Ito, H., Fujimoto, K., Tanaka, H., Lockner, D. (Eds.), Proceedings of the International Workshop on the Nojima Fault Core and Borehole Data Analysis. Preliminary Report, pp. 147–152.

Logan, J.M., Dengo, C.A., Higgs, N.G., Wang, Z.Z., 1992. Fabrics of experimental fault zones: their development and relationship to mechanical behaviour. In: Evans, B., Wong, T.-F. (Eds.). Fault Mechanics and Transport Properties of Rocks. Academic Press, London, pp. 33–67.

Mandl, G., de Jong, L.N.J., Maltha, A., 1977. Shear zones in granular material. Rock Mechanics 9, 95–144.

Mase, C.W., Smith, L., 1987. Effects of frictional heating on the thermal, hydrological, and mechanical response of a fault. Journal of Geophysical Research 92, 6249–6272.

McCaig, A.M., 1988. Deep fluid circulation in fault zones. Geology 16, 867–870.

Miller, S.A., 2002. The properties of large ruptures and the dynamical influence of fluids and seismicity and faulting. Journal of Geophysical Research, submitted for publication.

Mizoguchi, K., Hirose, T., Shimamoto, T., 2000. Permeability structure of the Nojima fault at Funaki, Hokudan-cho, Japan. Gekkanchikyu-gougai (Earth Monthly) 31, 58–65 (in Japanese).

Morrow, C.A., Lockner, D.A., 1994. Permeability differences between surface-derived and deep drillhole core samples. Geophysical Research Letters 21, 2151–2154.

Morrow, C.A., Shi, L.Q., Byerlee, J.D., 1984. Permeability of fault gouge under confining pressure and shear stress. Journal of Geophysical Research 89, 3193–3200.

Muir-Wood, R., 1994. Earthquakes, strain-cycling and the mobilization of fluids. In: Parnell, J. (Ed.), Geofluids: Origin, Migration and Evolution of Fluids in Sedimentary Basins. Geological Society Special Publication 78, pp. 99–112.

Ohtomo, Y., 1993. Origin of the Median Tectonic Line. Journal of Science of the Hiroshima University 9, 611–669.

Rice, J.R., 1992. Fault stress states, pore pressure distributions and the weakness of the San Andreas fault. In: Evans, B., Wong, T.-F. (Eds.). Earthquake Mechanics and Transport Properties of Rocks. Academic Press, London, pp. 475–503.

Rutter, E.H., Maddock, R.H., Hall, S.H., White, S.H., 1986. Comparative microstructures of natural and experimentally produced clay-bearing fault gouges. Pure and Applied Geophysics 124, 3–30.

Sakakibara, N., 1995. Structural evolution of multiple ductile shear zone system in the Ryoke belt, Kinki Province. Journal of Science of the Hiroshima University 10, 267–332.

Sammis, C.G., Osborne, R.H., Anderson, J.L., Banerdt, M., White, P., 1986. Self-similar cataclasis in the formation of fault gouge. Pure and Applied Geophysics 124, 53–78.

Schulz, S.E., Evans, J.P., 2000. Mesoscopic structure of the Punchbowl Fault, Southern California and the geologic and geophysical structure of active strike-slip faults. Journal of Structural Geology 22, 913–930.

Seront, B., Wong, T.-F., Caine, J.S., Forster, C.B., Bruhn, R.L., Fredrich, J.T., 1998. Laboratory characterization of hydrodynamical properties of a seismogenic normal fault system. Journal of Structural Geology 20, 865–881.

Shimada, K., Takagi, H., Osawa, H., 1998. Geotectonic evolution in transpressional regime: time and space relationships between mylonitization and folding in the southern Ryoke belt, eastern Kii Peninsula, southwest Japan. Journal of the Geological Society of Japan 104, 825–844 (in Japanese with English abstract).

Shimamoto, T., Takemura, K., Fujimoto, K., Tanaka, H., Wibberley, C.A.J., 2001. Nojima fault zone probing by core analyses—preface to Part II. The Island Arc 10, 357–359.

Sibson, R.H., 1973. Interactions between temperature and pore-fluid pressure during earthquake faulting and a mechanism for partial or total stress relief. Nature 243, 66–68.

Sibson, R.H., 1986. Brecciation processes in fault zones: inferences from earthquake rupturing. Pure and Applied Geophysics 124, 159–175.

Sibson, R.H., 1992. Implications of fault valve behaviour for rupture nucleation and recurrence. Tectonophysics 211, 283–293.

Sugiyama, Y., 1992. Neotectonics of the forearc zone and the Setouchi Province in southwest Japan. Memoir of the Geological Society of Japan 40, 219–223 (in Japanese with English abstract).

Tadokoro, K., Nishigami, K., Ando, M., Hirata, N., Iidaka, T., Hashida, Y., Shimakaki, K., Ohmi, S., Kano, Y., Koizumi, M., Matsuo, S., Wada, H., 2001. Seismicity changes related to a water injection experiment in the Nojima Fault zone. The Island Arc 10, 235–243.

Takagi, H., 1985. Mylonitic rocks of the Ryoke belt in the Kayumi area, eastern part of the Kii Peninsula. Journal of the Geological Society of Japan 91, 637–651 (in Japanese with English abstract).

Takagi, H., 1986. Implications of mylonitic microstructures for the geotectonic evolution of the Median Tectonic Line, central Japan. Journal of Structural Geology 8, 3–14.

Takagi, H., Shibata, K., Sugiyama, Y., Uchiumi, S., Matsumoto, A., 1989. Isotopic ages of rocks along the Median Tectonic Line in the Kayumi area, Mie Prefecture. Journal of Petrology, Mineralogy and Economic Geology 84, 75–88 (in Japanese with English abstract).

Tchalenko, J.S., 1968. The evolution of kink-bands and the development of compression textures in sheared clays. Tectonophysics 6, 159–174.

Teufel, L.W., 1987. Permeability changes during shear deformation of fractured rock. 28th US Symposium of Rock Mechanics, pp. 473–480.

Walsh, J.B., 1981. Effect of pore pressure and confining pressure on fracture permeability. International Journal of Rock Mechanics, Mining Science and Geomechanics Abstracts 18, 429–435.

Zhang, S., Cox, S.F., 2000. Enhancement of fluid permeability during shear deformation of a synthetic mud. Journal of Structural Geology 22, 1385–1393.

Zhu, W., Wong, T.-f., 1997. The transition from brittle faulting to cataclastic flow: permeability evolution. Journal of Geophysical Research 102, 3027–3041.

Zoback, M.D., Byerlee, J.D., 1975a. The effect of microcrack dilatancy on the permeability of Westerly granite. Journal of Geophysical Research 80, 752–755.

Zoback, M.D., Byerlee, J.D., 1975b. Permeability and effective stress. American Association of Petroleum Geologists Bulletin 59, 154–158.